2021 American Control Conference (ACC)
New Orleans, USA, May 25-28, 2021

Robust Control of the Flywheel Inverted Pendulum System Considering Parameter Uncertainty

Amir Ali Amiri Moghadam and Matthew Marshall[1]

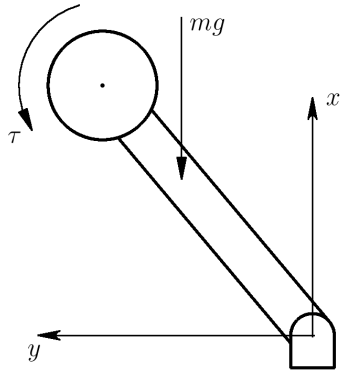

Fig. 1. Conceptual flywheel inverted pendulum

***Abstract*— A linear controller for the unstable flywheel inverted pendulum (also known as a reaction wheel inverted pendulum or inertia wheel pendulum) is designed using Quantitative Feedback Theory (QFT) to provide response that stays withing upper and lower bounds in the face of significant variations of the plant parameters. A mathematical model of the plant, including both the mechanics of the pendulum and the electromechanics of the motor, is derived. Simulation is used to compare performance of the QFT controller to that of simple PID compensation. It is shown that while the QFT controller consistently satisfies the robust performance bounds for all plant uncertainty in both frequency and time domains, the PID controller fails to provide robust tracking performance.**

I. INTRODUCTION

The conceptual flywheel inverted pendulum (FIP) is shown in Fig. 1. It is in unstable equilibrium when the rod is vertical. Actuation comes via the torque, τ, applied between the pendulum rod and the flywheel.

The flywheel inverted pendulum has numerous potential applications in systems that require balancing. For example, it has been investigated for a cube that can stand either on an edge or a point [1], a robot unicycle [5], and a robot bicycle [2]. Also, the rotational inertia of a humanoid robot's torso is modeled as a flywheel in various locomotion schemes [3]. In these applications it could be expected that the parameters of the pendulum model would differ from those for which the controller was designed. Consider that the pendulum rod inertia would vary in the robot-bicycle application with riders of different mass or for the bipedal-robot if it were laden with extra equipment. Damping at the pendulum axis would vary with changing ground conditions. Despite the quotidian nature of these uncertainties, little work has been done to account for them in controller design. The effects of variations in rod length, flywheel mass, and flywheel mass moment of inertia on system response have been investigated but the results are used to determine advantageous parameters for FIP design [4]. A linear time-variant model of the FIP is used to account for the changing rod length when a humanoid robot transitions from bipedal to quadrupedal locomotion [6]. All other parameters are treated as known values. In order to bolster the applicability of the flywheel inverted pendulum to practical systems, the present work studies its control in the presence of significant parameter uncertainty.

The quantitative feedback theory (QFT) can generate controllers that are robust to parameter changes. Within the literature there are several contributions for control of the flywheel inverted pendulum system. Olivares and Albertos have designed a PID controller and a linear controller in the outer loop to provide global stability for the system [11]. Montoya and Gonzáles have used Lyapunov's method to design a nonlinear controller for flywheel inverted pendulum system [12]. Rizal et al. have acquired sliding mode control for robust control of the FIP [13]. In the current work we propose application of QFT for robust position control of the FIP system considering parameter uncertainty. Horowitz initially introduced QFT as a robust feedback control design technique [4]. This technique has been further developed by Horowitz and others [14], [15], [16]. In most frequency domain robust control methods such as H_∞ the controller design procedure is only based on the magnitude of the transfer function. However, QFT not only takes into account the magnitude information, but also considers the phase information in the design process [7]. The main advantage of the QFT method is that it can allow direct controller design based on robust performance bounds.

Governing equations for the FIP model under consideration are derived in §II, resulting in a transfer function having rod angle as its output and applied motor voltage as input. In §III, transient-response targets are identified for the FIP and the design of a suitable QFT controller is described. The behavior of this closed-loop system is compared to one with PID compensation, both in the nominal case and for cases where motor parameters vary. Concluding remarks and proposed direction for future work are provided in §IV.

II. PLANT MODEL

The differential equations relating the pendulum angle and the voltage applied to the motor are developed and

[1] Amir Ali Amiri Moghadam (aamirimo@kennesaw.edu) and Matthew Marshall (mqm@kennesaw.edu) are with the Department of Robotics and Mechatronics Engineering, Kennesaw State University, Kennesaw, GA 30144, USA

978-1-6654-4197-1/$31.00 ©2021 AACC

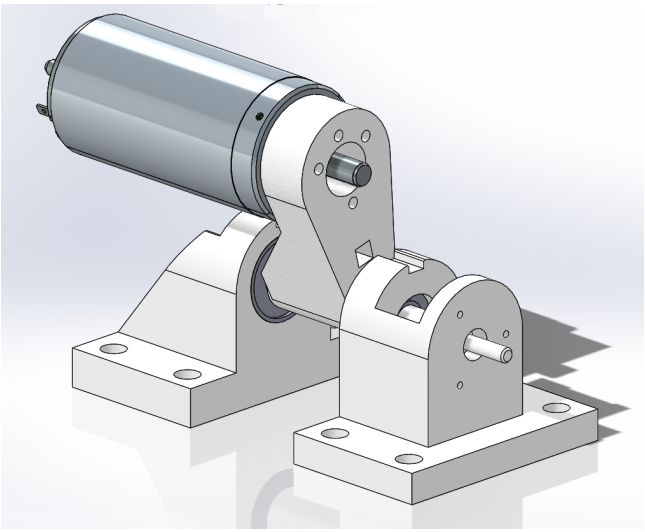

Fig. 2. CAD representation of FIP under consideration, fasteners and encoder not shown

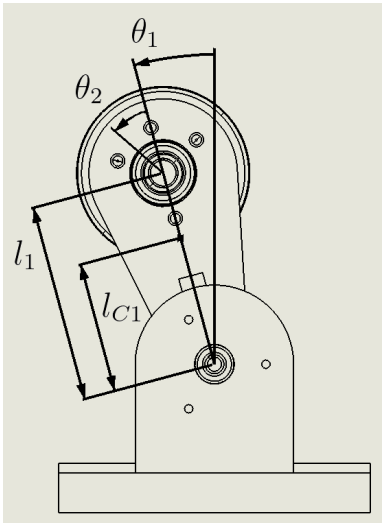

Fig. 3. Displacement parameters for flywheel inverted pendulum model

the resulting transfer function is presented. Derivations of a flywheel-inverted-pendulum mathematical model can be found in numerous other works [17] but since a substantial number are incorrect, the transfer function is derived afresh here.

A depiction of the plant is given in Fig. 2. It comprises an electric motor, optical encoder (not shown), 3D-printed components,[2] bearings, and fasteners (also not shown). The motor is a Maxon brushed 90 watt model. The armature of this motor provides sufficient rotational inertia so an additional flywheel is not needed. Neither the motor-shaft position nor its speed are measured. The angle of the pendulum rod is sensed with a Maxon five hundred counts-per-turn optical quadrature encoder. The two base parts and the pendulum rod are 3D printed. They are connected through a pair of 608ZZ ball bearings. The shaft protruding from the base part on the right in Fig. 2 is part of the printed pendulum rod and is what the encoder connects to.

The displacement parameters for the FIP are shown in Fig. 3. The angular displacement of the pendulum rod from vertical is denoted with θ_1. The displacement of the motor shaft from a position aligned with the pendulum rod is denoted with θ_2. The distance between the pendulum axis and the motor shaft is given as l_1 and the distance between the pendulum axis and the center of mass of the rod is l_{C1}.

Applying Newton's second law for rotation to the pendulum rod and combining it with the results of applying Newton's second law (for translation) to the motor armature yields

$$\left(m_1 l_{C1} + m_2 l_1\right)\left(g S_1\right) - b_1\dot{\theta}_1 + b_2\dot{\theta}_2 - \tau_m = \left(J_1 + m_2 l_1^2\right)\ddot{\theta}_1 \tag{1}$$

where m_i is the mass of the i-th link (in this case the pendulum rod and the motor), g is the gravitational acceleration constant, S_1 denotes the sine of the pendulum-rod angle, b_i is the viscous damping of the i-th joint, τ_m is the motor torque, and J_1 is the mass moment of inertia of the pendulum rod about the axis of rotation.

Applying Newton's second law for rotation to the motor yields

$$\tau_m - b_2\dot{\theta}_2 = J_{C2}\left(\ddot{\theta}_1 + \ddot{\theta}_2\right) \tag{2}$$

where J_{C2} is the mass moment of inertia of the motor about its center of mass (in this case, its axis).

Combining (1) and (2) with the electromechanical equations for a brushed motor yields the governing equations for the FIP. The motor voltage, current, speed, and torque are related by

$$\begin{aligned} e_a &= R_a i_a + e_b \\ e_b &= K_b\dot{\theta}_2 \\ \tau_m &= K_t i a \end{aligned}$$

where e_a is the voltage applied to the armature, R_a is the armature resistance, i_a is the armature current, e_b is the back EMF, K_b is the back-EMF constant, and K_t is the torque constant.

The values for the flywheel inverted pendulum modeled here are

$$\begin{aligned} l_1 &= 40.0 \text{ mm}, \quad l_{C1} = 19.2 \text{ mm}, \\ m_1 &= 22.4 \text{ g}, \quad m_2 = 340 \text{ g}, \\ b_1 &= 62\ \mu\text{N}\cdot\text{m}\cdot\text{s} \quad b_2 = 6.2\ \mu\text{N}\cdot\text{m}\cdot\text{s} \\ J_1 &= 16.1 \text{ kg}\cdot\text{mm}^2, \quad J_{C2} = 6.96 \text{ kg}\cdot\text{mm}^2, \\ K_b &= 52.5 \text{ mV}\cdot\text{s}, \quad K_t = 52.5 \text{ mN}\cdot\text{m}\cdot\text{A} \\ R_a &= 2.07\ \Omega, \quad \text{and} \quad L_a = 0.620 \text{ mH}. \end{aligned}$$

The armature inductance, L_a, is left out of the analysis because the quotient

[2]CAD files are available at https://github.com/DrMattMarshall/flywheel_inverted_pendulum

$$\frac{L_a}{R_a} = \frac{0.62 \text{ mH}}{2.07\ \Omega}$$

is more than one order of magnitude smaller than the 5 ms time constant of the motor. Combining the motor equations yields

$$\tau_m = -\left(\frac{K_b K_t}{R_a}\right)\dot{\theta}_2 + \left(\frac{K_t}{R_a}\right)e_a$$

Substituting this into (1) and (2) results in

$$J_{C2}\left(\ddot{\theta}_1 + \ddot{\theta}_2\right) = -\rho\dot{\theta}_2 + \nu e_a \quad (3)$$

$$\frac{1}{\phi}\ddot{\theta}_1 = \gamma S_1 - b_1\dot{\theta}_1 + \rho\dot{\theta}_2 - \nu e_a \quad (4)$$

where $\rho \equiv \frac{K_b K_t}{R_a} + b2$, $\nu \equiv \frac{K_t}{R_a}$, $\phi \equiv \frac{1}{J_1 + m_2 l_1^2}$, and $\gamma \equiv (m_1 l_{C1} + m_2 l_1)\, g$.

Substituting (4) into (3) then rearranging gives the governing equations

$$\ddot{\theta}_1 = \gamma\phi S_1 - b_1\phi\dot{\theta}_1 + \phi\rho\dot{\theta}_2 - \nu\phi e_a \quad (5)$$

$$\ddot{\theta}_2 = -\gamma\phi S_1 + b_1\phi\dot{\theta}_1 - \rho\zeta\dot{\theta}_2 + \nu\zeta e_a \quad (6)$$

where $\zeta \equiv \frac{1}{J_{C2}} + \phi$. Applying the small-angle approximation to S_1 in (5) and (6), taking the Laplace transform of them, and then solving for $\frac{\Theta_2(s)}{E_a(s)}$ yields the plant transfer function.

$$P(s) = \frac{\nu\phi s}{s^3 + (b_1\phi + \rho\zeta)\, s^2 + (\phi)\left(\frac{b_1\rho}{J_{C2}} - \gamma\right) s - \frac{\gamma\phi\rho}{J_{C2}}}$$

$$= \frac{1570s}{s^3 + 278s^2 - 135s - 1.66 \times 10^5}$$

This is a third-order system with one unstable pole.

III. CONTROL DESIGN AND ANALYSIS

In this section, the design of a robust controller using QFT for robust position of the flywheel inverted pendulum system is presented. In practice, it is very difficult to obtain robust stability and tracking performance for open-loop systems that have parameter uncertainty. Designing a single robust controller that can guarantee the robust performance of the system despite the variation in the system parameters is therefore advantageous. QFT is a robust control design technique which is proposed by Horowitz [7], [8].

The QFT controller control design procedure can be summarized as follows. Firstly, the variation of the system parameters at fixed frequencies will be obtained. (This is called the plant template.) Secondly, the robust performance bounds will be calculated based on the design requirement and the templates. Finally, a nominal open-loop system will be designed in way that satisfies all robust performance bounds (loop shaping). Fig. 4 shows the two-degree-of-freedom feedback structure of QFT design. In this figure, $P(s,\epsilon)$ is the plant with uncertainty, $G(s)$ is the robust controller, and $F(s)$ is the prefilter.

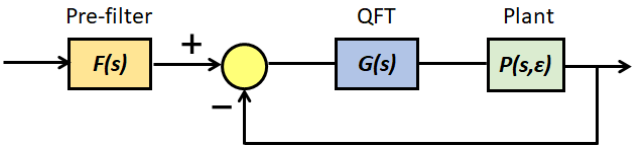

Fig. 4. Block diagram of plant with QFT compensation

The main objective of this section is to design a robust controller and prefilter such that the system is stable and can track desired inputs. The robust stability specification is defined as follows [9].

$$\left|\frac{P(s,\epsilon)G(s)}{1 + P(s,\epsilon)G(s)}\right| < 1.2$$

The robust tracking specification is defined as

$$\alpha(s) \le \left|\frac{F(s)P(s,\epsilon)G(s)}{1 + P(s,\epsilon)G(s)}\right| \le \beta(s)$$

where $\alpha(s)$ and $\beta(s)$ are systems that define the upper and lower tracking bound of the system.

The robust tracking bounds usually are defined by second order systems. However, to widen the bounds at high frequencies and reduce the cost of feedback we can add one zero to the upper bound and one pole to the lower bound [9]. For the FIP, the desired tracking specifications are selected as 20% overshoot and settling time of 40 ms. These performance goals are selected arbitrarily, but the controller-design process would be the same with different values. Future, experimental work can be performed to revisit the matter of realistic tracking specifications. The resulting robust tracking bounds are:

$$\alpha(s) = \frac{32.39(s + 1500)}{s^2 + 200s + 48100}$$

$$\beta(s) = \frac{1.429 \times 10^7}{(s + 300)(s + 219.3)^2}$$

Both transfer functions have settling time of forty seconds, $\alpha(s)$ is underdamped (with overshoot of 20%) and $\beta(s)$ is critically damped.

In order to calculate the robust performance bounds based on the design requirement, one needs to generate the plant template based on the system uncertainty. In the current work, 100% uncertainty is considered in the electric motor parameters K_b, K_t, R_a, J_{C2}, and m_2. Fig. 5 shows the computed boundary of plant templates, that is, the variation of gain and phase of transfer functions relative to the nominal transfer function at each design frequency, for the flywheel inverted pendulum system.

The robust performance bounds plus the nominal open loop system are shown in Fig. 6. In it, the stability bounds and tracking bounds at each design frequency are the black lines, while the blue line is the nominal open loop plant and the circles on this line refer to the design frequencies. To design a QFT controller each circle needs to be above its associated tracking bound and outside of the closed contours

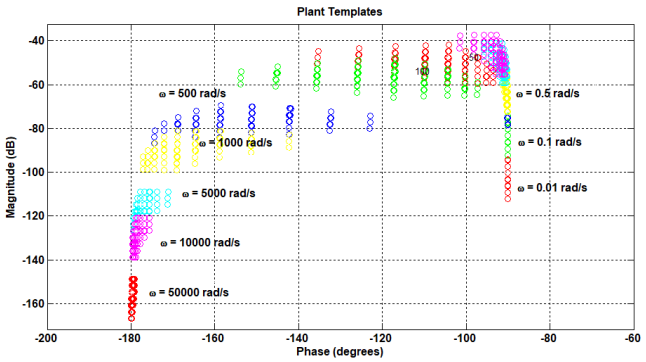

Fig. 5. The boundary of the plant template — system response at different frequencies and parameter variations

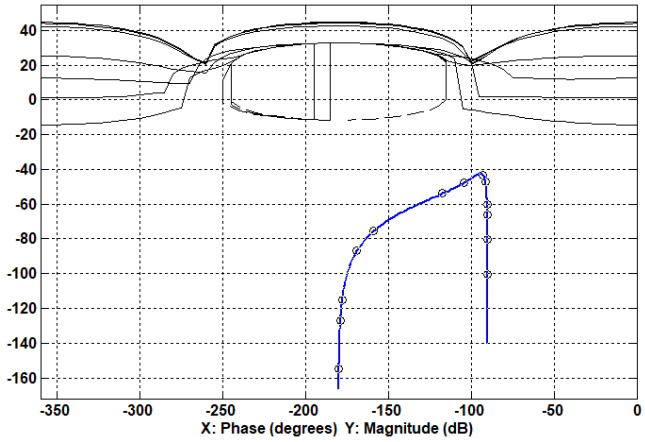

Fig. 6. Robust performance bounds (black) and nominal open-loop system (blue) on the Nichols chart

of the stability bounds. It is apparent from this figure a controller is needed. Loop shaping is applied [10] to obtain a controller that satisfies these requirements. The result is shown in Fig. 7. The robust controller associated with this figure is

$$G(s) = \frac{\left(8440 \times 10^6\right)(s+164.2)(s+29.08)(s+0.01498)}{(s^2)(s+3.521)(s+4663)}$$

and the prefilter transfer function is

$$F(s) = \frac{6.659(s+5330)}{(s+371.5)(s+97.00)}$$

To evaluate the robust tracking performance of the fly-wheel inverted pendulum system both its frequency and time domain responses are analyzed. Fig. 8 shows the bode plot of the open loop and closed loop (e.g., under QFT controller) systems for all considered plant uncertainty. Fig. 8b shows the frequency response of the closed loop system under QFT controller for all considered uncertainty. The red and green lines depict the desired robust tracking bounds. The effects of the zero added to $\alpha(s)$ and extra pole in $\beta(s)$ can be seen by the divergence of these two lines at higher frequencies. The figure shows that closed loop system exactly lies between the

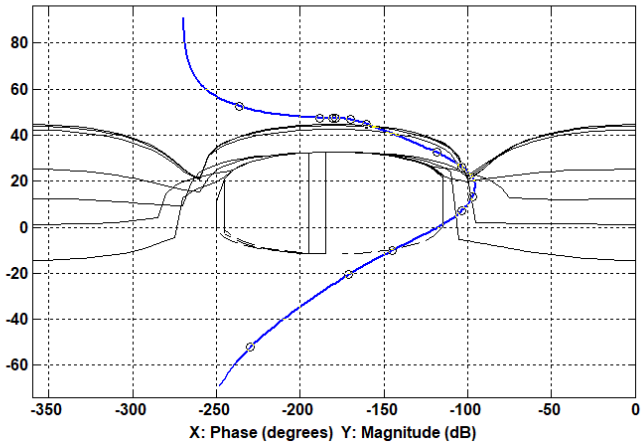

Fig. 7. Robust performance bounds (black) and result of loop shaping (blue) on the Nichols chart

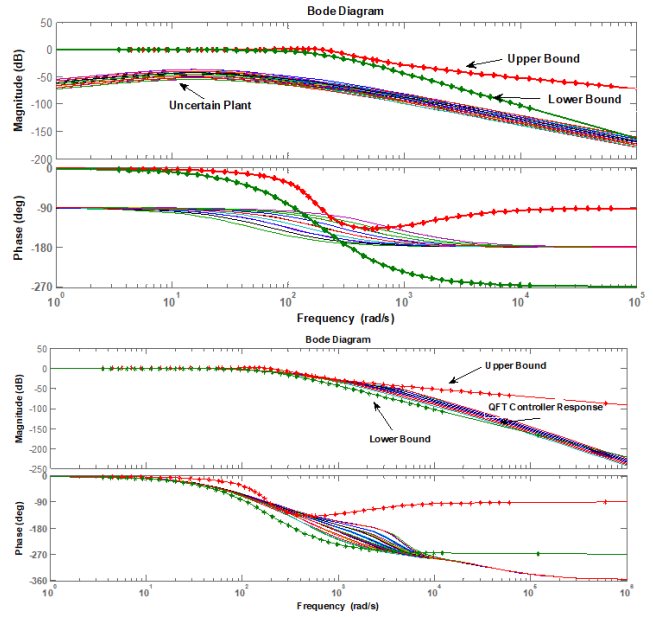

Fig. 8. Frequency response of (a) the open loop system for all considered plant uncertainty, and (b) the closed loop system under QFT controller for all considered plant uncertainty plus the desired upper and lower tracking bounds

robust tracking bounds for all considered uncertainty, which confirms the successful design of the QFT controller in the frequency domain.

To further analyze the performance of the QFT controller its step response is compared with that of a PID controller. The transfer function of this compensator is

$$G_{\text{PID}}(s) = \frac{9.960s^2 + 2680s + 160000}{s}$$

Fig. 9 shows the step response of the QFT and PID controllers for the nominal plant, and it can be seen that both controllers satisfy the tracking performances in terms of overshoot and settling time; neither rises above the top dashed line, which is 120% of the steady-state value, and both remain within 5% of steady-state after 40 ms.

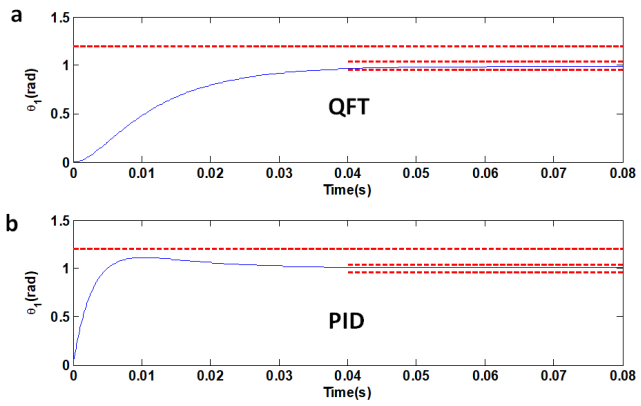

Fig. 9. Step response of QFT and PID controllers for nominal plant

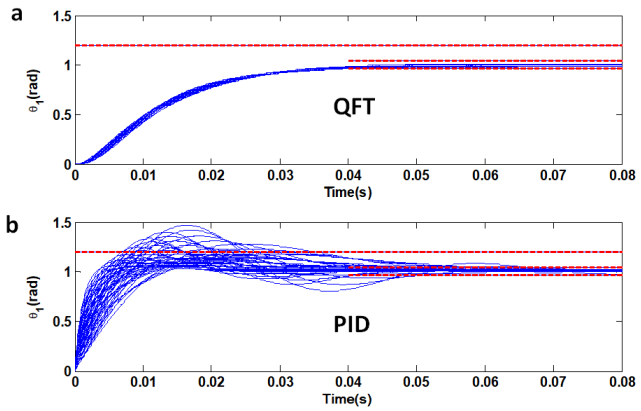

Fig. 10. Step response of QFT and PID controllers for all considered parameter uncertainties of the motor

To assess the performance of these two controllers in the presence of plant variation, their step responses were simulated for changes in the plant motor parameters mentioned above. Fig. 10 shows the step response of both the QFT and PID controllers for all considered parameter uncertainty of the electromotor. According to this figure, the QFT controller robustly satisfies the tracking specifications, whereas the PID controller cannot reach the tracking performance target in terms of either overshoot or settling time.

IV. CONCLUSION AND FUTURE WORK

Using Newtonian mechanics, the dynamic model of the flywheel inverted pendulum is derived. This model includes the inertial dynamics of the pendulum as well as the dynamics of the electric motor. As a source of uncertainty in the system, the electric-motor parameters are considered to vary by 100%. Next, a robust controller using QFT is designed to guarantee the robust tracking performance of the system. Performance of the QFT controller is analyzed both in terms of bode plot and step response. Comparison of the QFT controller with a conventional PID controller indicates that while the QFT controller successfully satisfy the desired robust tracking specification, a PID controller cannot effectively compensate the effect of parameter uncertainty in the system.

Several lines of inquiry remain for characterizing the suitability of the QFT for controlling an FIP. It could be compared to compensators other than PID. Experimentation can be performed to assess the suitability of a QFT controller when implemented outside of simulation. For example — how does the magnitude of QFT control action compare to other compensators? does it robustly deal with the non-zero sampling period of a discrete-time system? what about quantization in a digital system? — are all questions of interest for implementing a stabilization scheme for the FIP.

REFERENCES

[1] M. Gajamohan, M. Muehlebach, T. Widmer and R. D'Andrea, "The Cubli: a reaction wheel based 3D inverted pendulum," 2013 European Control Conference (ECC), Zurich, 2013, pp. 268–274, doi: 10.23919/ECC.2013.6669562.

[2] K. Kanjanawanishkul, "LQR and MPC controller design and comparison for a stationary self-balancing bicycle robot with a reaction wheel," Kybernetika. 54. 173–191. 10.14736/kyb-2015-1-0173.

[3] J. Pratt, J. Carff, S. Drakunov, and A. Goswami, "Capture point: a step toward humanoid push recovery," in Humanoid Robots, 2006 6th IEEE-RAS International Conference on. IEEE, 2006, pp. 200–207.

[4] Q. K. Ho and C. B. Pham, "Study on inertia wheel pendulum applied to self-balancing electric motorcycle," 2018 4th International Conference on Green Technology and Sustainable Development (GTSD), Ho Chi Minh City, 2018, pp. 687–692, doi: 10.1109/GTSD.2018.8595698.

[5] X. Ruan, J. Hu and Q. Wang, "Modeling with Euler-Lagrange equation and cybernetical analysis for a unicycle robot," 2009 Second International Conference on Intelligent Computation Technology and Automation, Changsha, Hunan, 2009, pp. 108–111, doi: 10.1109/ICICTA.2009.263.

[6] T. Kamioka, T. Watabe, M. Kanazawa, H. Kaneko and T. Yoshiike, "Dynamic gait transition between bipedal and quadrupedal locomotion," 2015 IEEE/RSJ International Conference on Intelligent Robots and Systems (IROS), Hamburg, 2015, pp. 2195–2201, doi: 10.1109/IROS.2015.7353671.

[7] K. Torabi and A. A. Amiri Moghadam, "Robust control of conjugated polymer actuators considering the spatio-temporal dynamics," Proc. Inst. Mech. Eng. Part I J. Syst. Control Eng., vol. 226, no. 6, pp. 806–822, Jul. 2012, doi: 10.1177/0959651811435299.

[8] A.-A. Amiri-M, M. R. Gharib, M. Moavenian, and K. Torabiz, "Modelling and control of a SCARA robot using quantitative feedback theory," Proc. Inst. Mech. Eng. Part I J. Syst. Control Eng., vol. 223, no. 7, pp. 919–928, Nov. 2009, doi: 10.1243/09596518JSCE733.

[9] B. Azvine and R.J. Wynne, "A review of quantitative feedback theory as a robust control system design technique," Transactions of the Institute of Measurement and Control 14, no. 5, pp. 265–79, Dec. 1992, doi: 10.1177/014233129201400507.

[10] O. Yaniv, Quantitative Feedback Design of Linear and Nonlinear Control Systems (The Springer International Series in Engineering and Computer Science), New York, Kluwer Academic Pub1ishers, 1999.

[11] M. Olivares and P. Albertos, "On the linear control of underactuated systems: The flywheel inverted pendulum," in IEEE International Conference on Control and Automation, ICCA, 2013, pp. 27–32, doi: 10.1109/ICCA.2013.6564905.

[12] O. D. Montoya and W. Gil-González, "Nonlinear analysis and control of a reaction wheel pendulum: Lyapunov-based approach," Eng. Sci. Technol. an Int. J., vol. 23, no. 1, pp. 21–29, Feb. 2019, doi: 10.1016/j.jestch.2019.03.004.

[13] Y. Rizal, R. Mantala, S. Rachman, and N. Nurmahaludin, "Balance control of reaction wheel pendulum based on second-order sliding mode control," in Proceedings - 2018 International Conference on Applied Science and Technology, iCAST 2018, 2018, pp. 51–56, doi: 10.1109/iCAST1.2018.8751548.

[14] I. M. Horowitz, Synthesis of Feedback Systems. New York: Academic Press, 1963.

[15] M. Sidi and I. M. Horowitz, "Synthesis of feedback systems with large plant ignorance for prescribed time domain tolerances," in IFAC Proceedings Volumes, 1973, vol. 6, no. 2, pp. 202–206, doi: 10.1016/s1474-6670(17)68188-6.
[16] I. Horowitz and M. Sidi, "Optimum synthesis of non-minimum phase feedback systems with plant uncertainty," Int. J. Control, vol. 27, no. 3, pp. 361–386, 1978, doi: 10.1080/00207177808922376.
[17] M. Spong, P. Corke, and R. Lozano, "Nonlinear control of the reaction wheel pendulum," Automatica, vol. 37, no. 11, pp. 1845–1851, doi: 10.1016/S0005-1098(01)00145-5.